



Fabrication of halloysite nanotubes/polypyrrole nanocomposites for efficient removal of methyl orange

Mengmeng Zhang^{a,*}, Liangliang Chang^b, Zehao Yu^a

^aState Key Laboratory Breeding Base of Nuclear Resources and Environment, School of Chemical Biology and Materials Science, East China University of Technology, Nanchang 330013, Jiangxi, China, Tel./Fax: +86 0791 83896550; emails: zhangmmnpu@163.com (M. Zhang), yzh0426@foxmail.com (Z. Yu)

^bCollege of Chemical Engineering and Modern Materials, Shaanxi Key Laboratory of Comprehensive Utilization of Tailings Resources, Shangluo University, Shangluo 726000, Shaanxi, China, Tel./Fax: +86 0914 2312156; email: chang_liang_100@126.com

Received 12 November 2017; Accepted 16 March 2018

ABSTRACT

Halloysite nanotubes/polypyrrole (HNTs/PPy) nanocomposites were fabricated by in situ polymerization of pyrrole monomer in the presence of HNTs. The structures of the composites were analyzed by X-ray diffraction, Fourier transform infrared spectra, thermogravimetric analysis and transmission electron spectroscopy. Subsequently, the capability of HNTs/PPy nanocomposites on the removal of methyl orange from aqueous solution was systematically studied. The HNTs/PPy nanocomposites showed high adsorption capacity toward methyl orange and a maximum adsorption capacity of 214.6 mg/g at 25°C was achieved. The adsorption kinetics demonstrated a rapid methyl orange uptake by HNTs/PPy and the experimental data were well fitted to the pseudo-second-order model. The Langmuir and Freundlich models were employed to describe the adsorption isotherms, and the results presented that the equilibrium data obeyed both the Langmuir and Freundlich models. Thermodynamic parameters of ΔG° and ΔH° verified the spontaneous and exothermic nature of the methyl orange adsorption onto HNTs/PPy. Furthermore, the regeneration experiments revealed that HNTs/PPy nanocomposites could be reused after treated with hydrochloric acid solution, showing potential applications in purification of dyeing effluents.

Keywords: Halloysite nanotubes; Polypyrrole; Adsorption; Methyl orange

1. Introduction

Various kinds of dyes effluents, generated from dyeing, textile, leather, paper and other related industries, have become a rising global environmental concern. The discharge of dyes effluents into receiving streams even at very low concentrations can cause serious pollution to the environment [1–3]. Wastewaters containing dyes are toxic to aquatic life and may cause health problems to human beings, such as kidney disease, damage to nervous system, genetic mutation, cancer and so on. In addition, the presence of color dyes in waters also decreases the amount of light penetration, thus hindering photosynthesis of aquatic plants and increasing the chemical

oxygen demand [4,5]. Therefore, it is of great importance to remove dyes pollutants from effluents before their final discharging into the environment. Most dye molecules contain benzene ring structure and they are especially resistant to oxidation and biodegrade, which makes the treatment of dyes wastewaters more difficult.

Many attempts have been made for removing dyes from wastewaters, such as membrane separation, flocculation precipitation, oxidation, photocatalytic degradation, microbial degradation and adsorption [6–9]. Among these techniques, adsorption is commonly used because of its advantages such as high efficiency, low cost and simple in operation [10,11]. And the selection of adsorbent with large adsorption

* Corresponding author.

capacity, high efficiency and low cost is the key issue in adsorption technique. In the recent years, natural, cheap and non-secondary pollution materials used as adsorbents have attracted increasing attentions.

Halloysite nanotubes ($\text{Al}_2\text{Si}_2\text{O}_5(\text{OH})_4$; HNTs) are a kind of natural aluminosilicate clay with a predominantly hollow tubular structure. They possess multilayer walls with Si–OH on the external surface and Al–OH on the internal surface [12]. HNTs have been applied in numerous applications such as medicine, drug delivery, biomaterial, nanocomposites, catalysts and adsorbents, owing to their beneficial characteristics of abundant resources, environmentally friendly, large surface area, plentiful micropores and high porosity [13–17]. As adsorbents, HNTs have been studied to remove dyes [18], Cr(VI) [19] and Pb(II) [20]. For instance, Liu et al. [21] reported that the HNTs exhibited high adsorption capacity toward methyl violet and the maximum adsorption capacity for methyl violet was 113.64 mg/g. Chiew et al. [22] prepared halloysite/alginate nanocomposite beads and used them as adsorbents to remove Pb^{2+} from wastewater. The results showed that the nanocomposite beads removed Pb^{2+} via physisorption and ion exchange, and a very high adsorption capacity of 325 mg/g for Pb^{2+} was achieved. Li et al. [23] synthesized halloysite@polyaniline hybrid via a one-step facile procedure. And the fabricated hybrid was found to be an effective adsorbent for adsorption of Cr(VI) oxyanion with a maximum adsorption capacity of 62.9 mg/L. Hebbbar et al. [24] investigated the influence of HNTs functionalized with polydopamine on the adsorption performance. The resulting composites exhibited significantly improved adsorption performance of Pb^{2+} and Cd^{2+} . The above researches reveal that HNTs used as adsorbents for contaminants removal are usually modified in order to improve their adsorption capacity. Therefore, it is necessary to develop new and facile techniques to functionalize halloysite nanotubes with aim to effectively enhance their adsorption properties.

Polypyrrole (PPy) is one of the most important conducting polymers. It has been intensively researched due to its high electrical conductivity, non-toxicity, high flexibility, easy preparation, low cost and good stability [25–27]. These unique properties of PPy make it good candidate for many applications such as batteries, super capacitor, electromagnetic shielding, electrocatalysis, biological materials and so on [28–31]. Especially, it is found that there exists some positively charged nitrogen atoms in the PPy chains. To maintain charge neutrality, PPy will absorb anionic ions in aqueous solutions through ions exchange and electrostatic interactions, which shows a good prospect for its applications in the removal of anionic contaminants from aqueous solution [32]. However, pure PPy displays a low adsorption capacity and has a tendency to aggregate by π – π interaction, resulting in the insufficient use of PPy. To solve this problem, the fabrication of PPy nanocomposites is expected to be an effective way to overcome the aggregation of PPy and to increase its adsorption capacity. Li et al [33] reported PPy/ TiO_2 for methylene blue removal in aqueous solution, suggesting that the adsorption capacity of PPy/ TiO_2 was about 5.5 times higher than that of pure PPy. Shafiabadi et al. [34] synthesized PPy/SBA-15 nanocomposites for Hg(II) adsorption and observed a maximum adsorption capacity of 200 mg/g. Setshedi et al. [35] prepared PPy/graphene oxide nanocomposite and noted that

its adsorption capacity for Cr(VI) is much higher than that of traditional PPy. The preparation of PPy nanocomposites and their application in heavy metals removal have been widely studied, and HNTs/PPy composites have previously been prepared and used for the removal of Cr(VI) [36,37]. Moreover, the HNTs/PPy composites have much potential as effective adsorbents for almost all anionic dyes, owing to their innate cationic nature. However, HNTs/PPy nanocomposites have never been used for the removal of anionic dyes. Therefore, in this work, HNTs were incorporated into PPy to prepare the HNTs/PPy composites via in situ polymerization method. Then, the HNTs/PPy composites used as adsorbent for methyl orange removal in aqueous solution was studied. Methyl orange, a water-soluble azo dye, was chosen as a model anionic dye because of its toxicity, dark color and carcinogenicity. The effects of adsorbent dose, initial concentration of methyl orange, contact time and temperature on the adsorption efficiency were investigated. Furthermore, the kinetic, isotherms and thermodynamics for the adsorption process were also evaluated.

2. Experimental

2.1. Reagents and materials

HNTs were purchased from Henan Tianfu Fine Chemical Co., Ltd. (Zhengzhou, China). Methyl orange was purchased from Shanghai Meryer Chemical Technology Co., Ltd. (Shanghai, China). Ferric chloride hexahydrate was purchased from Tianjin Baishi Chemical Co., Ltd. (Tianjin, China). Ethanol was purchased from Tianjin Fuyu Fine Chemical Co., Ltd. (Tianjin, China). Polyvinylpyrrolidone (PVP) was purchased from Sinopharm Chemical Reagent Co., Ltd. (Beijing, China). Pyrrole was purchased from Aladdin Industrial Corporation (Shanghai, China). Hydrochloric acid was purchased from Infinity Scientific Co., Ltd. (Beijing, China). Distilled water was made by our laboratory.

2.2. Preparation of halloysite nanotubes/polypyrrole nanocomposite

The HNTs/PPy composites were prepared via in situ polymerization. HNTs (1.0 g), distilled water (60.0 mL) and PVP (0.2 g) were added into a 250 mL three-mouth flask, followed by ultrasonication for 30 min. The flask was then kept in an ice bath to cool down with mechanical stirring. Then, pyrrole monomer (1 mL) was added into the flask through a syringe. After 30 min, 30 mL of $\text{FeCl}_3 \cdot 6\text{H}_2\text{O}$ solution (1 mol/L), used as oxidizing agent, was added dropwise to the flask through a constant pressure funnel. Then, the reaction mass was kept below 5°C with stirring at which the polymerization continued for 8–10 h. After that, the mixture was filtered and washed with ethanol and distilled water. Finally, the black powder was obtained and dried at 60°C for 12 h under vacuum. The product was abbreviated HNTs/PPy, and the loading percentage of the PPy is about 40%–45%.

2.3. Characterization

Fourier transform infrared (FTIR) spectrum was recorded between 400 and 4,000 cm^{-1} with a resolution of 2 cm^{-1} on a Nicolet FTIR 5700 spectrometer (USA).

X-ray diffraction (XRD) tests were carried out by using a X'Pert Pro MPD diffractometer (PANalytical, Holland) with Cu K α radiation ($\lambda = 0.154178$ nm). The tube voltage was 36 kV, and the current was 20 mA. Scans were taken over the 2θ range of 5° – 80° with the scanning rate of $0.02^\circ/\text{s}$.

Thermal gravimetric analysis (TGA) tests were carried out by using Perkin Elmer TGA-7 (USA) at a heating rate of $20^\circ\text{C}/\text{min}$ in a nitrogen atmosphere.

Transmission electron microscopic (TEM) tests were carried out by a H-7650 transmission electron microscope operating at 200 kV.

2.4. Adsorption experiments

Adsorption experiment was performed by adding 0.025–0.15 g of HNTs/PPy nanocomposites to conical flasks, into which 50 mL methyl orange solutions were added, respectively. The initial concentrations of methyl orange varied from 30 to 300 mg/L. After adding HNTs/PPy, the conical flasks were shaken in a thermostatic shaker for 120 min. Then, the methyl orange solution was filtered to get the filtrate. The methyl orange concentration of filtrate was tested by a UV-vis spectrophotometer (UV-2550, Japan) at λ of 463 nm, which is identified as the equilibrium concentration of methyl orange (C_e). The removal efficiency, adsorption capacity of methyl orange adsorbed by HNTs/PPy nanocomposites at time (q_t , mg/g) and at equilibrium (q_e , mg/g) was obtained by Eqs. (1)–(3), respectively.

$$R = \frac{C_0 - C_t}{C_0} \times 100\% \quad (1)$$

$$q_t = \frac{(C_0 - C_t)V}{m} \quad (2)$$

$$q_e = \frac{(C_0 - C_e)V}{m} \quad (3)$$

where C_0 , C_t and C_e are the initial, t time and equilibrium concentrations of methyl orange (mg/L), respectively; V is the volume of methyl orange solution (L); m is the mass of HNTs/PPy adsorbent used (g).

2.5. Regeneration experiments

Regeneration of HNTs/PPy nanocomposites was studied by adsorption/desorption experiments. First, 0.05 g of HNTs/PPy was used to absorb 50 mL of 150 mg/L methyl orange solution for 50 min. Then, 0.05 g of used adsorbent was treated with 50 mL of HCl solution (1 mol/L) for desorption. After 1 h, the treated adsorbents were separated and washed with distilled water. Finally, the regenerated HNTs/PPy nanocomposites were reused to absorb 50 mL of 150 mg/L methyl orange solution to test their recyclability.

3. Results and discussions

3.1. FTIR analysis of HNTs/PPy nanocomposites

The structures and surface functional groups of HNTs and HNTs/PPy nanocomposites were studied by FTIR.

Fig. 1(a) shows the FTIR spectrum of the HNTs. It can be seen the HNTs show peaks at 3,695, 3,620 and 3,449 cm^{-1} , which are attributed to the stretching vibrations of hydroxyl groups. The peak at 1,092 cm^{-1} is ascribed to the stretching vibration of Si–O bond. The peak shown at 912 cm^{-1} is the bending vibration of hydroxyl groups. The peaks shown at 534 and 468 cm^{-1} are caused by the bending vibrations of Al–O and Si–O bonds, respectively. The FTIR spectrum of HNTs/PPy nanocomposites (Fig. 1(b)) shows much difference from that of HNTs. The peak at 1,642 cm^{-1} is assigned to the bending vibration of N–H groups. The peaks at 1,545 and 1,452 cm^{-1} are considered the stretching vibrations of pyrrole ring. Peaks at 1,039 and 911 cm^{-1} are attributed to C–H bending vibrations and C–H deformations, respectively. These results confirmed the presence of PPy in the nanocomposite.

3.2. XRD analysis of HNTs/PPy nanocomposites

The structures of HNTs and HNTs/PPy nanocomposites were further examined by XRD. The pure HNTs (Fig. 2(a)) exhibit diffraction peaks at $2\theta = 11.8^\circ, 19.9^\circ, 24.4^\circ, 29.8^\circ, 34.9^\circ, 38.2^\circ, 54.7^\circ$ and 62.4° , which are the characteristic peaks of crystalline HNTs. And the results are well consistent with the earlier published XRD pattern of HNTs [38]. In the case of HNTs/PPy nanocomposites (Fig. 2(b)), the diffraction peaks of HNTs can also be observed in the nanocomposites without any appreciable shift in the diffraction angles, suggesting that the PPy polymerization onto HNTs' surface did not disturb the crystalline structure of HNTs. While compared with HNTs, the peak intensities for HNTs/PPy nanocomposites obviously reduced, which is related to the coating of the amorphous PPy onto HNTs.

3.3. Thermal properties of HNTs/PPy nanocomposites

The thermogravimetric curves of HNTs and HNTs/PPy composites vs. temperature at the heating rate of $20^\circ\text{C}/\text{min}$

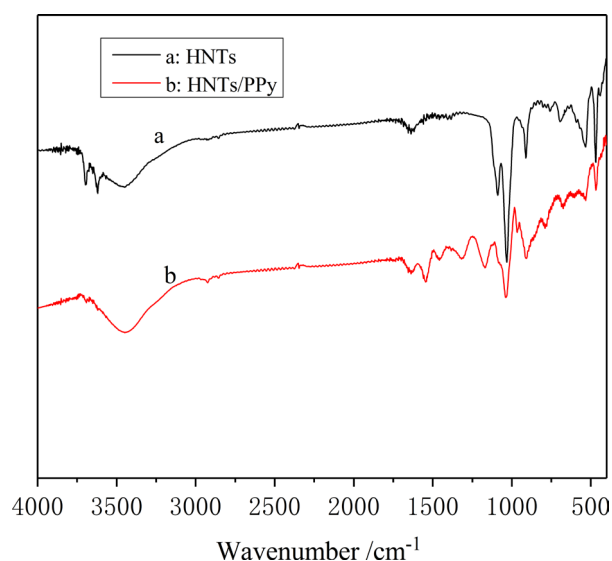


Fig. 1. FTIR spectra of HNTs (a) and HNTs/PPy nanocomposite (b).

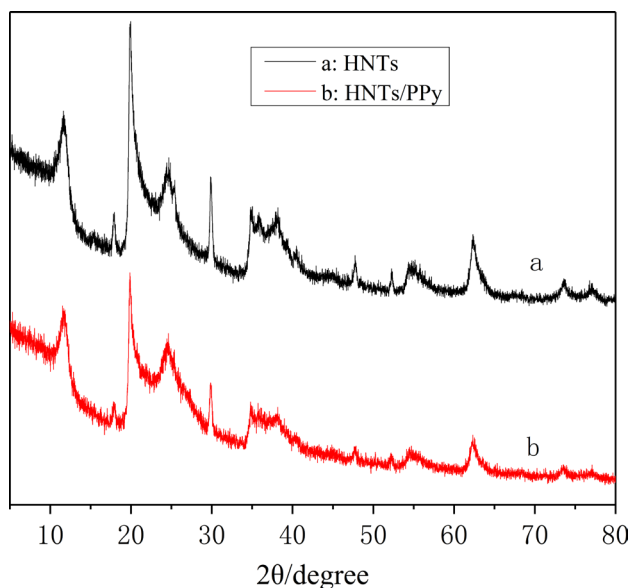


Fig. 2. XRD spectra of HNTs (a) and HNTs/PPy nanocomposite (b).

are displayed in Fig. 3. It can be seen from Fig. 3(a) that the HNTs are thermally stable. The mass loss below 150°C is attributed to the removal of absorbed water. The mass loss of HNTs is rapid at 435°C, and the major mass loss of 10.11% in the range of 435°C–535°C is attributed to the dehydroxylation of the residual structural aluminol groups in HNTs. For the HNTs/PPy nanocomposites (as shown in Fig. 3(b)), the degradation temperature is lower than that of HNTs from 25°C to 800°C, and the char residue at 800°C is also much lower than that of HNTs, which is caused by the thermal decomposition of PPy in the nanocomposites.

3.4. TEM analysis of HNTs/PPy nanocomposites

TEM was used to characterize the morphologies of HNTs and HNTs/PPy nanocomposites, and the images are shown in Fig. 4. It can be seen that the pure HNTs (Fig. 4(a)) exhibit a hollow and open-ended structure with very smooth surfaces. While the morphology of the HNTs/PPy nanocomposites (Fig. 4(b)) is quite different from that of the pure HNTs. Many dark deposits on the surface of nanotubes can be observed, which is attributed to the PPy layer attached onto the HNTs surface from outside. To sum up, the analysis results of FTIR, XRD, TGA and TEM show that the HNTs/PPy composites are successfully synthesized.

3.5. Effect of adsorbent dosage

The effect of the adsorbent dose on adsorption was studied by adding different amounts of HNTs/PPy nanocomposites (from 0.025 to 0.15 g) in 50 mL 90 mg/L methyl orange solution at 25°C with stirring for 120 min, and the results are shown in Fig. 5. It can be seen that the removal efficiency of methyl orange increases from 75.4% to 98.6% with the adsorbent dose increasing from 0.025 to 0.15 g. This behavior is ascribed to the fact that there are more available active adsorption sites for methyl orange to adhere by increasing

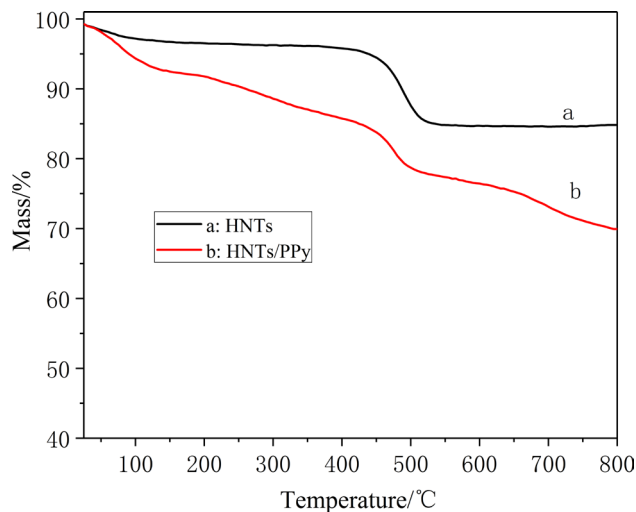


Fig. 3. Overlay TGA curves of HNTs (a) and HNTs/PPy nanocomposite (b).

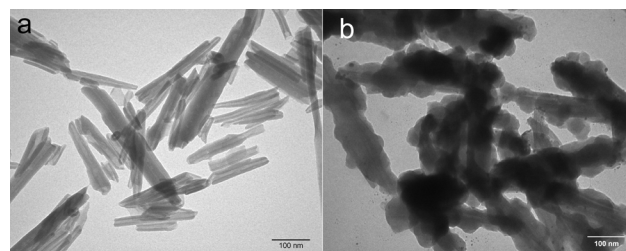


Fig. 4. TEM images of HNTs (a) and HNTs/PPy nanocomposite (b).

adsorbent dosage, so the increase of HNTs/PPy dosage can improve the removal efficiency of methyl orange. However, the adsorption capacity reduces from 135.6 to 29.6 mg/g as the adsorbent dose increases from 0.025 to 0.15 g. With the adsorbent dosage increasing, HNTs/PPy nanocomposites tend to aggregate together at high concentration, and the aggregated nanotubes can create diffusion resistance for the adherence of methyl orange onto the adsorbents' surfaces, thus decreasing the adsorption capacity of methyl orange on HNTs/PPy. When the HNTs/PPy dosage is 0.05 g, the removal efficiency and adsorption capacity are 93.9% and 85.9 mg/g, respectively, and further increase of HNTs/PPy cannot significantly increase the removal efficiency because of the aggregation of HNTs/PPy. Consequently, the adsorbent dose of 0.05 g was considered as optimum dose to methyl orange removal in the following experiments.

3.6. Effect of contact time and initial methyl orange concentration

Fig. 6 shows the effect of contact time and initial concentration on adsorption capacity of methyl orange by HNTs/PPy with the adsorption condition of natural pH and 25°C. It can be seen that the HNTs/PPy composites exhibit very high adsorption rate in the first 20 min. At the initial stage of adsorption, the active adsorption sites on the surface of HNTs/PPy are vacant and the concentration gradient is high, so the methyl orange can be quickly adsorbed to the surfaces of HNTs/PPy. Afterwards, the active adsorption sites

on the HNTs/PPy surface are gradually occupied and the concentration gradient gradually decreases, so the adsorption rate gradually decreases with the increase of contact time until the adsorption reaches equilibrium. It is found that a minimum contact time of 50 min is enough to remove methyl orange from aqueous solution, so a contact time of 50 min is selected as the adsorption time in further experiments. In addition, it is also noted from Fig. 6 that an increase in initial methyl orange concentration leads to an increase in methyl orange uptake. Distinctively, the adsorption capacity of methyl orange at equilibrium increases from 85.9 to 178.9 mg/g by increasing the initial concentration of methyl orange from 90 to 210 mg/L. This is mainly attributed to the fact that the higher initial concentration can develop greater driving force to overcome the mass transfer resistance of methyl orange molecules between the aqueous and solid phases, therefore, the higher initial dye concentration results in higher adsorption capacity.

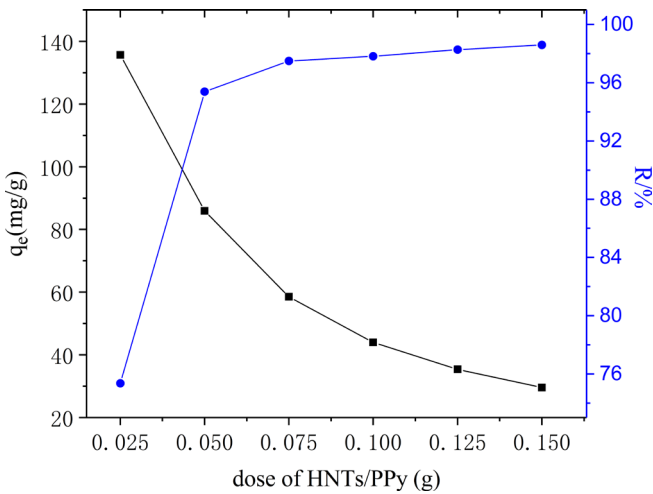


Fig. 5. Effect of HNTs/PPy dose on adsorption of methyl orange onto HNTs/PPy nanocomposite.

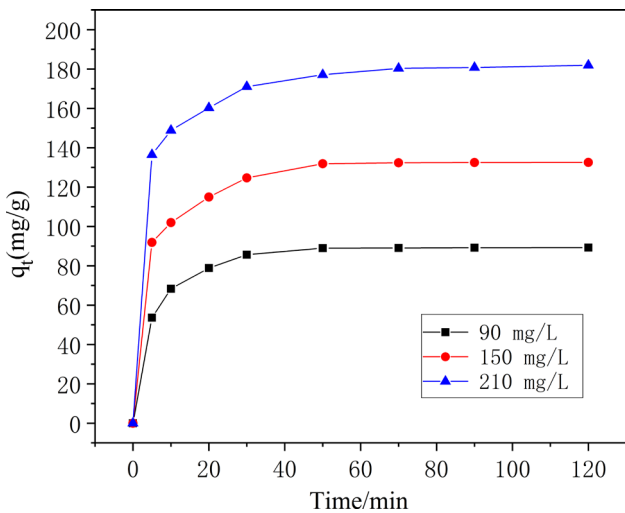


Fig. 6. Effect of contact time and initial methyl orange concentration on adsorption of methyl orange onto HNTs/PPy nanocomposite.

3.7. Effect of temperature and initial dye concentration

Temperature and initial dye concentration are important factors that affect the adsorption process. The effects of temperature and initial dye concentration on adsorption process were studied by adding 0.05 g HNTs/PPy into 50 mL methyl orange solutions with initial concentrations ranging from 30 to 300 mg/L at 25°C–45°C. Fig. 7 displays the adsorption capacities at different temperatures as a function of initial methyl orange concentration. The adsorption capacity of methyl orange onto HNTs/PPy is found to increase with the increasing initial methyl orange concentration from 30 to 300 mg/L, and the maximum adsorption capacities at 25°C, 35°C and 45°C are determined as 214.6, 213.5 and 215.3 mg/g, respectively. It is also noted that the adsorption capacities are almost the same at different temperatures, suggesting that the temperature can hardly affect the adsorption process of methyl orange onto HNTs/PPy. It may give more chance for HNTs/PPy nanocomposites to be use in practical adsorption application.

3.8. Adsorption kinetics of methyl orange adsorption onto HNTs/PPy nanocomposites

Adsorption kinetics is usually used to study the relations of adsorption capacity and time in the process of adsorption. In order to explore the mechanism and rate-controlling steps of the adsorption process, the pseudo-first-order Eq. (4), pseudo-second-order Eq. (5) and intra-particle diffusion Eq. (6) models are employed to predict adsorption kinetics in this experiment.

$$\lg(q_e - q_t) = \lg q_e - k_1 \frac{t}{2.303} \tag{4}$$

$$\frac{t}{q_t} = \frac{1}{k_2 q_e^2} + \frac{t}{q_e} \tag{5}$$

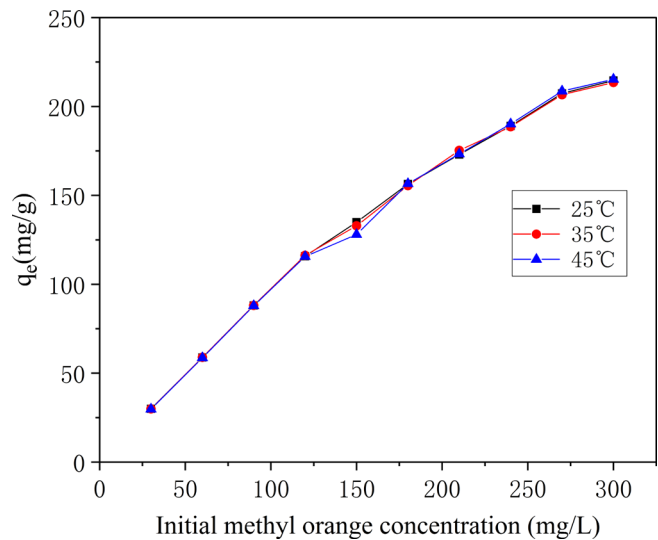


Fig. 7. Effect of temperature and initial methyl orange concentration on adsorption of methyl orange onto HNTs/PPy nanocomposite.

$$q_t = k_1 t^{0.5} + C \tag{6}$$

where q_e and q_t (mg/g) are the adsorption capacities at t time and equilibrium of methyl orange, respectively. k_1 (min^{-1}) and k_2 (g/mg·min) are the equilibrium rate constants of pseudo-first-order and pseudo-second-order, respectively. k_i (mg/g $\text{min}^{1/2}$) is the intra-particle diffusion constant.

Linear plots of $\lg(q_e - q_t)$ vs. t for the pseudo-first-order and t/q_t vs. t for the pseudo-second-order model are shown in Figs. 8 and 9, respectively. The kinetic parameters and correlation coefficients (R^2) calculated by the above linear plots are reported in Table 1. The correlation coefficients from pseudo-first-order model are low, in the range of 0.9540–0.9779. Besides, the calculated $q_{e,\text{cal}}$ (mg/g) values from pseudo-first-order model are far from the experimental values of $q_{e,\text{exp}}$ (mg/g). In contrast, the correlation coefficients (R^2) for the second-order kinetic model are all greater than 0.999, and

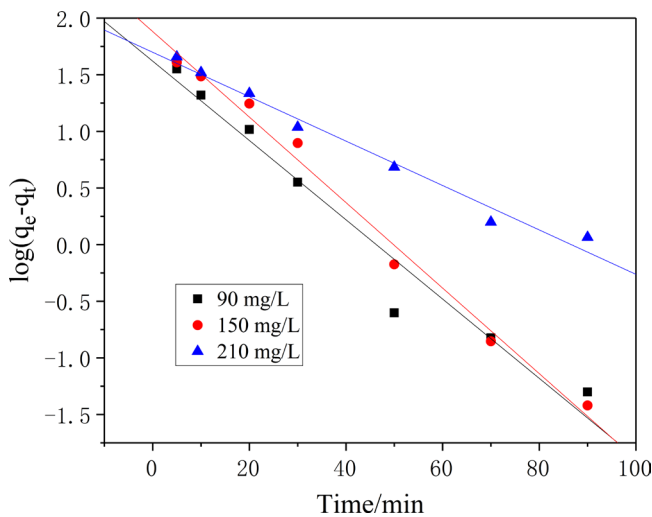


Fig. 8. The pseudo-first-order kinetic plots for methyl orange adsorption onto HNTs/PPy nanocomposite.

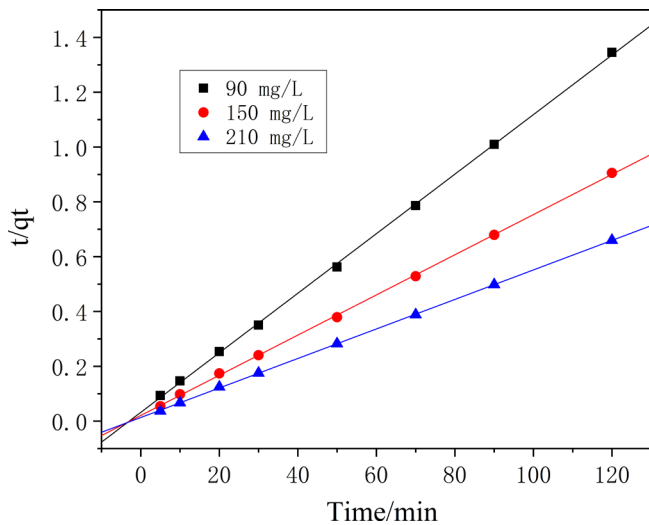


Fig. 9. The pseudo-second-order kinetic plots for methyl orange adsorption onto HNTs/PPy nanocomposite.

the calculated $q_{e,\text{cal}}$ (mg/g) values from pseudo-second-order model are very close to the experimental values of $q_{e,\text{exp}}$ (mg/g), which indicates that the pseudo-second-order model is more appropriate for describing the adsorption kinetics of methyl orange onto HNTs/PPy. The mechanism of the adsorption process is further studied by intra-particle diffusion model (Eq. (6)). Plots of q_t vs. $t^{0.5}$ are multilinear curves and do not pass through the origin, as shown in Fig. 10. This result indicates that the rate-determining step in the adsorption process is controlled by more than one mechanism such as intra-particle diffusion, chemical reaction, film diffusion and bulk diffusion [39].

3.9. Adsorption isotherms of methyl orange adsorption onto HNTs/PPy nanocomposites

Adsorption isotherms are very useful in describing the interactions between adsorbent and adsorbate, and investigating the adsorption mechanisms. The experimental data are fitted by Langmuir and Freundlich adsorption isotherm models.

Table 1
Adsorption kinetic parameters of methyl orange onto HNTs/PPy

Kinetic models	Methyl orange concentration (mg/L)		
	90	150	210
Pseudo-first-order			
$q_{e,\text{exp}}$ (mg/g)	85.9	132.6	178.9
$q_{e,\text{cal}}$ (mg/g)	41.7	76.1	49.9
k_1 (min^{-1})	0.0811	0.0872	0.0448
R^2	0.9540	0.9879	0.9779
Pseudo-second-order			
$q_{e,\text{cal}}$ (mg/g)	89.1	135.4	181.5
k_2 (g/mg·min)	0.0037	0.0017	0.0009
R^2	0.9996	0.9997	0.9999

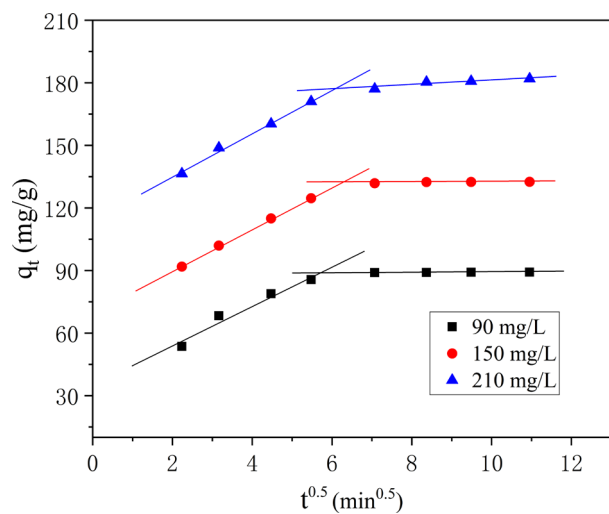


Fig. 10. The intra-particle diffusion model for methyl orange adsorption onto HNTs/PPy nanocomposite.

The Langmuir model is described by Eq. (7):

$$\frac{C_e}{q_e} = \frac{C_e}{q_m} + \frac{1}{K_L q_m} \quad (7)$$

where C_e (mg/L) is the equilibrium concentration of adsorbate, q_e (mg/g) is the adsorption capacity of adsorbate at equilibrium (mg/g), q_m (mg/g) is the maximum monolayer adsorption capacity, and K_L (L/mg) is the Langmuir constant which related to adsorbent' surface active sites and adsorption intensity. Langmuir adsorption model is based on the assumption of monolayer adsorption on a homogeneous adsorbent surface with no interactions between adsorbent molecules. Linear plots of C_e/q_e vs. C_e for Langmuir model are shown in Fig. 11. The related K_L values, q_m as well as correlation coefficients (R^2) calculated from the slope and intercept of the above plots, are listed in Table 2. The correlation coefficients of the Langmuir isotherms are high, in the range of 0.975–0.988, which suggests that the adsorption process can be described by Langmuir isotherm. The calculated

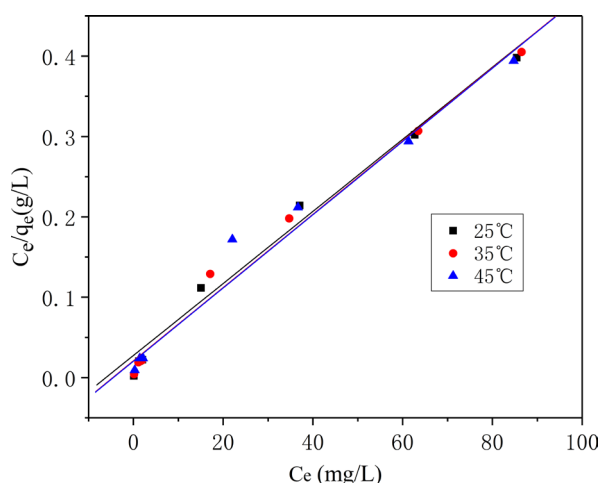


Fig. 11. Linear form for Langmuir isotherm model of methyl orange adsorption onto HNTs/PPy nanocomposite.

Table 2
Adsorption isotherm parameters of methyl orange onto HNTs/PPy

Isotherm models	Temperature (°C)		
	25	35	45
Langmuir			
q_m (mg/L)	219.8	219.8	223.2
K_L (L/mg)	0.221	0.211	0.162
R^2	0.988	0.988	0.975
R_L	0.0701–0.0149	0.0732–0.0156	0.0933–0.0202
Freundlich			
K_f (mg/g(mg/L) ^{1/n})	63.905	59.547	52.569
$1/n$	0.278	0.299	0.327
R^2	0.989	0.983	0.965

q_m values of HNTs/PPy are 219.8 mg/g at 25°C, 219.8 mg/g at 35°C and 223.2 mg/g at 45°C, respectively.

Furthermore, the dimensionless separation factor (R_L), which is an essential feature of the Langmuir isotherm, was studied to determine the favorability of an adsorption process. If the R_L value lies between 0 and 1, the adsorption process is favorable. The R_L value can be calculated from Eq. (8):

$$R_L = \frac{1}{1 + K_L C_0} \quad (8)$$

where K_L is the Langmuir constant (L/mg) and C_0 is the initial methyl orange concentration (mg/L).

The calculated R_L values are given in Table 2 and are all in the range of 0–1, indicating that the adsorption of methyl orange by HNTs/PPy is favorable.

The Freundlich model is described by Eq. (9):

$$\ln q_e = \ln K_f + \frac{1}{n} \ln C_e \quad (9)$$

where C_e (mg/L) is the equilibrium concentration of adsorbate, q_e (mg/g) is the adsorption capacity of adsorbate at equilibrium (mg/g). K_f (mg/g(mg/L)^{1/n}) and $1/n$ are Freundlich constants. K_f values are closely related to the properties and dosage of adsorbent, characteristics of adsorbate and environmental temperature, etc. The higher K_f value suggests higher affinity for methyl orange molecules. $1/n$ is related to the adsorption intensity. If the $1/n$ value lies between 0.1 and 1, the adsorption process is favorable. The Freundlich isotherm model is applicable for the adsorption on non-uniform surfaces and is not limited to the monolayer adsorption. Linear plots of $\ln q_e$ vs. $\ln C_e$ for Freundlich model are shown in Fig. 12 and the related Freundlich constants are shown in Table 2. The correlation coefficients (0.965–0.989) reveal that the experimental data also obey the Freundlich model. The $1/n$ values at 25°C, 35°C and 45°C are all in the range of 0.1–1, also indicating the adsorption process is favorable.

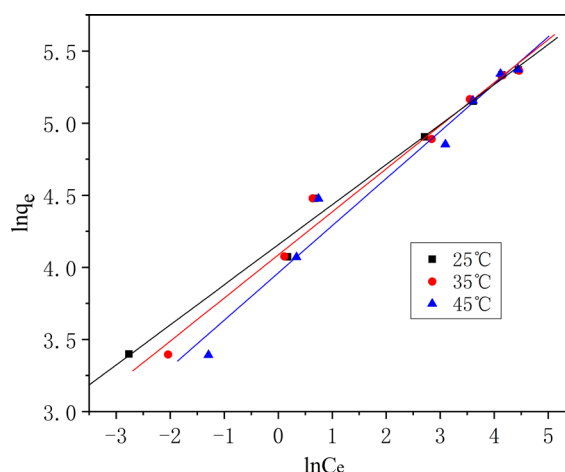


Fig. 12. Linear form for Freundlich isotherm model of methyl orange adsorption onto HNTs/PPy nanocomposite.

Table 3
Thermodynamic parameters of methyl orange adsorption onto HNTs/PPy

Temperature (K)	298	308	318
ΔG° (kJ/mol)	-27.72	-28.54	-28.76
ΔH° (kJ/mol)		-12.34	
ΔS° (J/mol·K)		52.10	

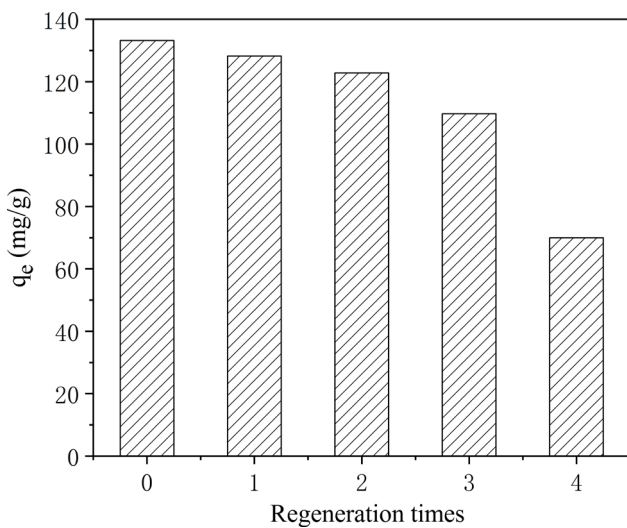


Fig. 13. Reusability stability of HNTs/PPy nanocomposites for methyl orange adsorption.

3.10. Thermodynamic parameters

In order to further study the mechanism of the adsorption process, the thermodynamic parameters including change in adsorption free energy (ΔG°), adsorption enthalpy (ΔH°) and adsorption entropy (ΔS°) are calculated by Eqs. (10) and (11):

$$\Delta G^\circ = -RT \ln K_L \quad (10)$$

$$\Delta G^\circ = \Delta H^\circ - T\Delta S^\circ \quad (11)$$

where K_L (L/mol) is the Langmuir constant, R (8.314 J/mol·K) is the gas constant; T (K) is the temperature. The ΔG° can be calculated from Eq. (10). ΔH° and ΔS° values can be calculated by the plot of ΔG° vs. T (figure not shown). All the calculated thermodynamic parameters are reported in Table 3. The negative ΔG° and ΔH° values indicate that the methyl orange adsorption is spontaneous and exothermic. While the positive value of ΔS° reveals that an increase in disorder at the solid–solution interface during the adsorption of methyl orange onto HNTs/PPy nanocomposites.

3.11. Regeneration of HNTs/PPy nanocomposites

To explore the regeneration ability of HNTs/PPy as adsorbent for removing methyl orange from aqueous solution,

desorption experiments were performed by using 1 M HCl solution as the desorbing agent. Fig. 13 shows the regeneration efficiency of HNTs/PPy undergoing four cycles of adsorption–desorption processes. It is noticed that the adsorption capacity reduces with the increase of adsorption–desorption cycles. The adsorption capacity of HNTs/PPy in the first three regeneration cycles all exceeds 100 mg/g, while the adsorption capacity decreases to 69 mg/g in the fourth cycle. The decrease in adsorption capacity may be ascribed to the fact that the methyl orange absorbed on HNTs cannot be completely desorbed after each cycle. The results suggest that the HNTs/PPy nanocomposites can be reused for at least three times for removing methyl orange in aqueous solution.

4. Conclusions

In this study, HNTs/PPy nanocomposites were synthesized, characterized and used for the removal of methyl orange from aqueous solution. The influence factors of adsorbent dose, contact time, initial methyl orange concentration and temperature on the adsorption efficiency were investigated. The results showed that the HNTs/PPy nanocomposites exhibited high adsorption rate toward methyl orange and the adsorption could reach equilibrium in 50 min. The adsorption data of kinetic were well fitted to the pseudo-second-order model. The results also presented that the isotherm data followed both the Langmuir and Freundlich models, and a maximum adsorption capacity was determined as 214.6 mg/g at 25°C. The thermodynamic analysis suggested that the adsorption process of methyl orange onto HNTs/PPy was spontaneous and exothermic. Moreover, the regeneration studies revealed that the HNTs/PPy could be reused for at least three times without considerable decrease of its adsorption capacity. Therefore, the fabricated HNTs/PPy is a promising adsorbent in the removal of methyl orange from wastewater owing to its high adsorption capacity, low cost and good stability.

References

- [1] J. Riu, I. Schönsee, D. Barceló, Determination of sulfonated azo dyes in groundwater and industrial effluents by automated solid-phase extraction followed by capillary electrophoresis/mass spectrometry, *J. Mass Spectrom.*, 33 (2015) 653–663.
- [2] R.V. Khandare, S.P. Govindwar, Phytoremediation of textile dyes and effluents: current scenario and future prospects, *Biotechnol. Adv.*, 33 (2015) 1697–1714.
- [3] N.R. Rane, V.V. Chandanshive, A.D. Watharkar, R.V. Khandare, T.S. Patil, P.K. Pawar, S.P. Govindwar, Phytoremediation of sulfonated remazol red dye and textile effluents by alternanthera philoxeroides: an anatomical, enzymatic and pilot scale study, *Water Res.*, 83 (2015) 271–281.
- [4] N. Song, X.L. Wu, S. Zhong, H. Lin, J.R. Chen, Biocompatible G-Fe₃O₄/CA nanocomposites for the removal of methylene blue, *J. Mol. Liq.*, 212 (2015) 63–69.
- [5] Ö. Şahin, M. Kaya, C. Saka, Plasma-surface modification on bentonite clay to improve the performance of adsorption of methylene blue, *Appl. Clay Sci.*, 2015, 116–117 (2015) 46–53.
- [6] S. Basak, N. Nandi, S. Paul, I.W. Hamley, A. Banerjee, A tripeptide-based self-shrinking hydrogel for waste-water treatment: removal of toxic organic dyes and lead (Pb²⁺) ions, *Chem. Commun.*, 53 (2017) 5910–5913.
- [7] T. Chidambaram, Y. Oren, M. Noel, Fouling of nanofiltration membranes by dyes during brine recovery from textile dye bath wastewater, *Chem. Eng. J.*, 262 (2015) 156–168.

- [8] P. Cooper, Removing colour from dyehouse waste waters – a critical review of technology available, *Color. Technol.*, 109 (2010) 97–100.
- [9] J. Wang, R. Li, Z. Zhang, X. Zhang, W. Sun, H. Wang, R. Xu, Z. Xing, Photocatalytic degradation of dyestuff wastewater under visible light irradiation using micron-sized mixed crystal TiO₂ powders, *J. Chem. Technol. Biotechnol.*, 82 (2007) 588–597.
- [10] K. Santhy, P. Selvapathy, Removal of reactive dyes from wastewater by adsorption on coir pith activated carbon, *Bioresour. Technol.*, 97 (2006) 1329–1336.
- [11] S.K. Gupta, N.M. Kumar, R. Misra, F.A. Ansari, D.D. Dionysiou, A. Maity, F. Bux, Synthesis and performance evaluation of a new polymeric composite for the treatment of textile wastewater, *Ind. Eng. Chem. Res.*, 55 (2015) 13–20.
- [12] M. Du, B. Guo, D. Jia, Newly emerging applications of halloysite nanotubes: a review, *Polym. Int.*, 59 (2010) 574–582.
- [13] W.T. Jiang, P.H. Chang, Y. Tsai, Z. Li, Halloysite nanotubes as a carrier for the uptake of selected pharmaceuticals, *Microporous Mesoporous Mater.*, 220 (2016) 298–307.
- [14] A. Philip, J. Lihavainen, M. Keinänen, T.T. Pakkanen, Gold nanoparticle-decorated halloysite nanotubes-selective catalysts for benzyl alcohol oxidation, *Appl. Clay Sci.*, 143 (2017) 80–88.
- [15] J. Jin, L. Fu, H. Yang, J. Ouyang, Carbon hybridized halloysite nanotubes for high-performance hydrogen storage capacities, *Sci. Rep.*, 5 (2015) 12429.
- [16] Q. Peng, M. Liu, J. Zheng, C. Zhou, Adsorption of dyes in aqueous solutions by chitosan-halloysite nanotubes composite hydrogel beads, *Microporous Mesoporous Mater.*, 201 (2015) 190–201.
- [17] K. Prashantha, H. Schmitt, M.F. Lacrampe, P. Krawczak, Mechanical behaviour and essential work of fracture of halloysite nanotubes filled polyamide 6 nanocomposites, *Compos. Sci. Technol.*, 71 (2011) 1859–1866.
- [18] M. Ghanbari, D. Emadzadeh, W.J. Lau, S.O. Lai, T. Matsuura, A.F. Ismail, Synthesis and characterization of novel thin film nanocomposite (TFN) membranes embedded with halloysite nanotubes (HNTs) for water desalination, *Desalination*, 358 (2015) 33–41.
- [19] X. Tian, W. Wang, Y. Wang, S. Komarneni, C. Yang, Polyethylenimine functionalized halloysite nanotubes for efficient removal and fixation of Cr (VI), *Microporous Mesoporous Mater.*, 207 (2015) 46–52.
- [20] D. Afzali, M. Fayazi, Deposition of MnO₂ nanoparticles on the magnetic halloysite nanotubes by hydrothermal method for lead(II) removal from aqueous solutions, *J. Taiwan Inst. Chem. Eng.*, 63 (2016) 421–429.
- [21] R. Liu, B. Zhang, D. Mei, H. Zhang, J. Liu, Adsorption of methyl violet from aqueous solution by halloysite nanotubes, *Desalination*, 268 (2011) 111–116.
- [22] C.S.C. Chiew, H.K. Yeoh, P. Pasbakhsh, K. Krishnaiah, P.E. Poh, B.T. Tey, E.S. Chan, Halloysite/alginate nanocomposite beads: kinetics, equilibrium and mechanism for lead adsorption, *Appl. Clay Sci.*, 119 (2016) 301–310.
- [23] C. Li, T. Zhou, H. Jin, Y. Lian, W. Han, Effective adsorption/reduction of Cr(VI) oxyanion by halloysite@polyaniline hybrid nanotubes, *ACS Appl. Mater. Interfaces*, 9 (2017) 6030–6043.
- [24] R.S. Hebbar, A.M. Isloor, K. Ananda, A.F. Ismail, Fabrication of polydopamine functionalized halloysite nanotube/polyetherimide membranes for heavy metal removal, *J. Mater. Chem. A*, 4 (2016) 764–774.
- [25] A.G. Macdiarmid, Polyaniline and polypyrrole: where are we headed? *Synth. Met.*, 84 (1997) 27–34.
- [26] J.O. Won-Ho, Y.H. Park, K.H. Kim, W.J. Bae, A water-soluble and self-doped conducting polypyrrole graft copolymer, *Macromolecules*, 38 (2015) 1044–1047.
- [27] M. Zhou, J. Heinze, Electropolymerization of pyrrole and electrochemical study of polypyrrole. 2. Influence of acidity on the formation of polypyrrole and the multipathway mechanism, *J. Phys. Chem. B*, 133 (1999) 8443–8450.
- [28] H.H. Chang, C.K. Chang, Y.C. Tsai, C.S. Liao, Electrochemically synthesized graphene/polypyrrole composites and their use in supercapacitor, *Carbon*, 50 (2012) 2331–2336.
- [29] C.Y. Huang, J.Y. Wu, K.Y. Tsao, C.L. Lin, C.P. Chang, C.S. Tsai, Y.H. Chen, J.T. Yeh, K.N. Chen, The manufacture and investigation of multi-walled carbon nanotube/polypyrrole/EVA nano-polymeric composites for electromagnetic interference shielding, *Thin Solid Films*, 519 (2011) 4765–4773.
- [30] D.H. Nam, K.S. Hong, S.J. Lim, M.J. Kim, H.S. Kwon, High-performance Sb/Sb₂O₃ anode materials using a polypyrrole nanowire network for Na-ion batteries, *Small*, 11 (2015) 2885–2892.
- [31] D. Wang, Y. Wang, X. Li, Q. Luo, J. An, J. Yue, Sunlight photocatalytic activity of polypyrrole-TiO₂ nanocomposites prepared by ‘in situ’ method, *Catal. Commun.*, 9 (2008) 1162–1166.
- [32] M. Bhaumik, A. Maity, V.V. Srinivasu, M.S. Onyango, Enhanced removal of Cr(VI) from aqueous solution using polypyrrole/Fe₃O₄ magnetic nanocomposite, *J. Hazard. Mater.*, 190 (2011) 381–390.
- [33] J. Li, J. Feng, W. Yan, Excellent adsorption and desorption characteristics of polypyrrole/TiO₂ composite for methylene blue, *Appl. Surf. Sci.*, 279 (2013) 400–408.
- [34] M. Shafiqabadi, A. Dashti, H.A. Tayebi, Removal of Hg (II) from aqueous solution using polypyrrole/SBA-15 nanocomposite: experimental and modeling, *Synth. Met.*, 212 (2016) 154–160.
- [35] K.Z. Setshedi, M. Bhaumik, M.S. Onyango, High-performance towards Cr(VI) removal using multi-active sites of polypyrrole-graphene oxide nanocomposites: batch and column studies, *Chem. Eng. J.*, 262 (2015) 921–931.
- [36] Y. Chao, L. Peng, Y. Zhao, Preparation and characterization of coaxial halloysite/polypyrrole tubular nanocomposites for electrochemical energy storage, *Electrochim. Acta*, 55 (2010) 6857–6864.
- [37] N. Ballav, H.J. Choi, S.B. Mishra, A. Maity, Polypyrrole-coated halloysite nanotube clay nanocomposite: synthesis, characterization and Cr(VI) adsorption behaviour, *Appl. Clay Sci.*, 102 (2014) 60–70.
- [38] Z. Shu, Y. Chen, J. Zhou, T. Li, D. Yu, Y. Wang, Nanoporous-walled silica and alumina nanotubes derived from halloysite: controllable preparation and their dye adsorption applications, *Appl. Clay Sci.*, 112–113 (2015) 17–24.
- [39] M.Y. Nassar, I.S. Ahmed, T.Y. Mohamed, M. Khatab, A controlled, template-free, and hydrothermal synthesis route to sphere-like α -Fe₂O₃ nanostructures for textile dye removal, *RSC Adv.*, 6 (2016) 20001–20013.

Supplementary material

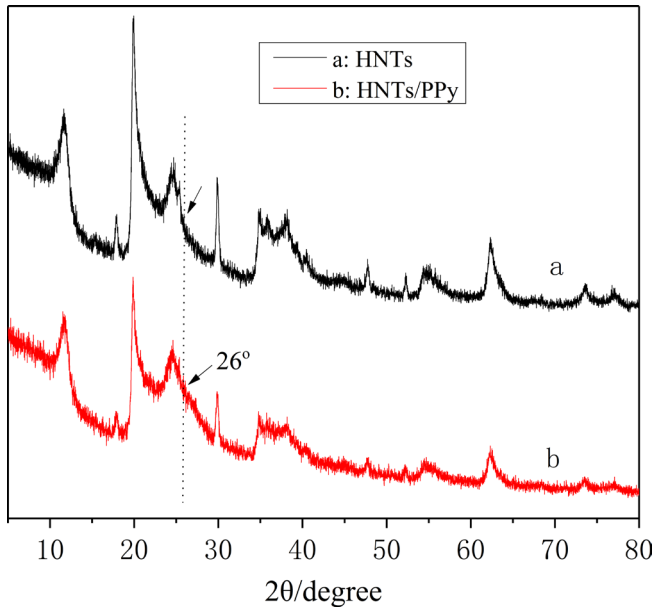


Fig. S1. Comparison of XRD spectra of HNTs (a) and HNTs/PPy nanocomposite (b).

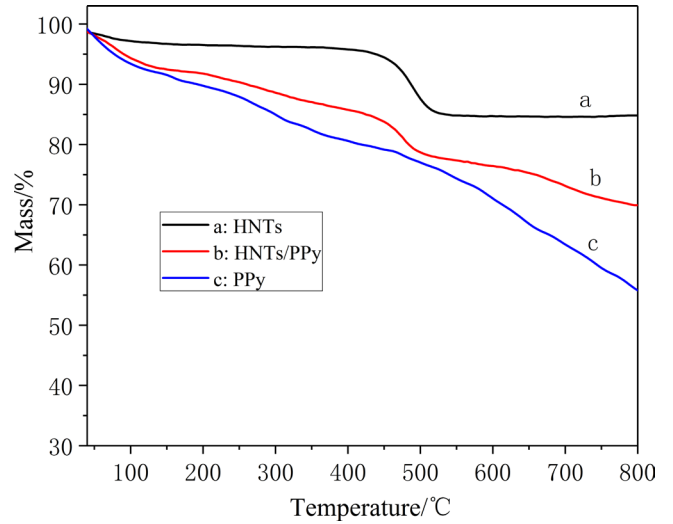


Fig. S2. TGA curves of HNTs (a), HNTs/PPy nanocomposite (b) and PPy (c).